Mon. Not. R. Astron. Soc. **320**, 435–444 (2001)

The Galactic disc distribution of planetary nebulae with warm dust emission features – II

S. Casassus[1,2] and P. F. Roche[1★]
[1]*Astrophysics, Physics Department, Oxford University, Keble Road, Oxford OX1 3RH*
[2]*Departamento de Astronomía, Universidad de Chile, Casilla 36-D, Santiago, Chile*

Accepted 2000 September 15. Received 2000 September 4; in original form 2000 March 17

ABSTRACT

We address the question of whether the distribution of warm-dust compositions in IR-bright Galactic disc PNe (Paper I, Casassus et al.) can be linked to the underlying stellar population. The PNe with warm dust emission represent a homogeneous population, which is presumably young and minimally affected by a possible dependence of PN lifetime on progenitor mass. The sample in Paper I thus allows testing of the predictions of single-star evolution, through a comparison with synthetic distributions and under the assumption that tip-of-the-AGB and PN statistics are similar. We construct a schematic model for AGB evolution (adapted from Groenewegen & de Jong), the free parameters of which are calibrated with the luminosity function (LF) of C stars in the LMC, the initial–final mass relation and the range of PN compositions. The observed metallicity gradient and distribution of star-forming regions with Galactocentric radius (Bronfman et al.) allow us to synthesize the Galactic disc PN progenitor population. We find that the fraction of O-rich PNe, $f(\mathrm{O})$, is a tight constraint on AGB parameters. For our best model, a minimum PN progenitor mass $M^{\min} = 1\,\mathrm{M}_{\odot}$ predicts that about 50 per cent of all young PNe should be O-rich, compared with an observed fraction of 22 per cent; thus $M^{\min} = 1.2\,\mathrm{M}_{\odot}$, at a 2σ confidence level ($M^{\min} = 1.3\,\mathrm{M}_{\odot}$ at 1σ). By contrast, current AGB models for single stars can account neither for the continuous range of N enrichment (Leisy & Dennefeld) nor for the observation that the majority of very C-rich PNe have Peimbert type I (Paper I). $f(\mathrm{O})$ is thus an observable quantity much easier to model. The decrease in $f(\mathrm{O})$ with Galactocentric radius, as reported in Paper I, is a strong property of the synthetic distribution, independent of $M^{\min}$. This trend reflects the sensitivity of the surface temperature of AGB stars and of the core mass at the first thermal pulse to the Galactic metallicity gradient.

Key words: stars: AGB and post-AGB – stars: evolution – ISM: abundances – planetary nebulae: general – infrared: ISM.

1 INTRODUCTION

The vertical stratification of planetary nebulae (PNe) according to their N/O abundance ratio (i.e., the Peimbert 1978 classification) is an indication that PN compositions can be linked to the masses of the progenitor. Yet few attempts have been taken at building a comprehensive picture of the distribution of PN chemical compositions in the Galactic context, although the range of C, N and O abundances has been successfully modelled (e.g. Kaler, Iben & Becker 1978; Renzini & Voli 1981; Bryan, Volk & Kwok 1990; Groenewegen, van den Hoek & de Jong 1995; Henry, Kwitter & Bates, 2000). The difficulties in PN population synthesis stem from an incomplete understanding of the late stages of stellar evolution, even for single stars on the asymptotic giant branch (AGB). Additionally, knowledge of the observational properties of PNe suffer from the lack of accurate distances, and the variety of object types and ages.

In Paper I (Casassus et al. 2001) we reported on the 8–13 μm dust features in catalogued compact and IR-bright Galactic disc PNe. The PNe with warm dust emission represent a homogeneous population: their maximum age is limited by the presence of dust close to the central star. The sample is thus minimally affected by a possible dependence of PN lifetime on progenitor mass (keeping in mind that selection effects in the direction of differential 'warm-dust' lifetimes as a function of grain composition are difficult to quantify; see section 6 in Paper I and Section 3 in this work). The dust-grain spectral signatures also provide a diagnostic of the C/O chemical balance, and an alternative to the gas-phase

★ E-mail: p.roche@physics.ox.ac.uk

abundances (e.g. Barlow 1983; Roche 1989). There is a trend for a decreasing fraction of O-rich PNe outside the solar circle, reflecting the decrease in the ratio of M to C stars found by Thronson et al. (1987) and Jura, Joyce & Kleinmann (1989).

Can the current scenarios for single-star evolution reproduce the observed frequencies of O- or C-rich grains in PNe, and the frequencies of Peimbert (1978) types among grain-types? Does the metallicity dependence of AGB evolution models predict the trends with Galactocentric radius? In this paper we analyse the Galactic distribution of PNe compositions in terms of simple stellar evolution models. We employ a set of analytical prescriptions in order to evolve stars with a continuous range of initial masses ($M_{\rm i}$, from 1 to 7 $\mathrm{M}_{\odot}$) and initial metallicity ($Z_{\rm i}$, from 0.005 to 0.035). This synthetic AGB model, coupled with a simple model for the Galactic disc, allows us to check whether single-star evolution can reproduce the distribution of PN chemical abundances.

We will conclude that the fractions of PNe displaying the dust signatures of O-rich and C-rich grains, $f(\mathrm{O}) + f(\mathrm{C}) = 1$, are tight constraints on the parameters of AGB evolution models. Synthetic AGB models that account for f(O) also reproduce the C-star luminosity function (LF) in the LMC, but the reverse is not true. However, for the PN sample analysed here, the minimum progenitor mass needs to be adjusted – our analysis favours a minimum progenitor mass of 1.2 $\mathrm{M}_{\odot}$ at 2σ. The Galactic f(O) gradient stems from the metallicity gradient, through the prescriptions for the core mass at the first thermal pulse and the AGB surface temperature. These results are an incentive to perfect the modelling, and pursue the use of PNe as probes of their progenitor population in different Galactic environments. Also, the advantage of PNe for testing AGB evolution models resides in their well-defined evolutionary status. For comparison, it is difficult to ascertain the thermally pulsing AGB membership of M stars, making the trends in the C/M star ratio much more difficult to model (see Section A2.1).

In Section 2 we present the procedure followed to synthesize the Galactic PN population, together with a brief description of the model used to evolve stars along the AGB (complete details are given in Appendix A). The free parameters in the AGB model were calibrated with observed quantities; this synthetic AGB model should thus be taken as an observational requirement rather than a detailed calculation. We investigate whether a model that reproduces the C-star LF in the LMC also reproduces f(O). Section 3 describes the process of linking the model results with the PN sample, the results of which will be presented in Section 4, together with an estimate of the minimum mass required to model the population of PNe with warm dust emission features. Section 5 contains a summary of our conclusions.

2 SYNTHETIC DISTRIBUTION OF PN COMPOSITIONS IN THE GALACTIC DISC

2.1 Synthetic AGB model

We aim at testing existing AGB evolution scenarios, such as that proposed by Groenewegen & de Jong (1993, hereafter GJ93). Synthetic AGB evolution models use empirical laws derived from detailed stellar evolution codes. As a starting point, we used GJ93, who follow Renzini & Voli (1981, hereafter, RV81) and include an explicit metallicity dependence whenever possible. Other models exist, like those of Bryan et al. (1990), Marigo, Bressan & Chiosi (1996) and Marigo, Girardi & Bressan (1999), but they have not been tested as extensively against observations as that of GJ93, which is also very light on computer resources and readily reproducible. The model is primarily concerned with the thermally pulsing AGB (TP-AGB), while the initial conditions at the start of the TP-AGB are functions of ($M_{\rm i}, Z_{\rm i}$).

The set of analytical prescriptions was taken from the compilation by GJ93, although we also considered a different treatment of hot bottom burning (HBB), making use of the results in Forestini & Charbonel (1997, hereafter FC97).[1] The free parameters which bear directly on f(O) are $\eta_{\rm AGB}$, the mass-loss parameter on the TP-AGB for a scaled Reimers (1975) law, and λ, the fraction of core growth between two consecutive thermal pulse that is dredged-up and mixed. We kept fixed the other parameters in GJ93: the minimum core mass for the third dredge-up, $M_{\rm c}^{\rm min} = 0.58\,\mathrm{M}_{\odot}$; the mass-loss parameter for the red giant branch, $\eta_{\rm RGB} = 0.86$; the mass-loss parameter for the early-AGB, $\eta_{\rm EAGB} = 3$.

The model was required to reproduce the C-star LF in the LMC and the initial–final mass relation for stars in the solar neighbourhood, as in GJ93 (Section A2). The best model, which fits the C-star LFs from Costa & Frogel (1996, hereafter CF96) and GJ93, corresponds to $\lambda = 0.75$, $\eta_{\rm AGB} = 4$, with a mass-loss rate high enough to keep the final masses within the observed limits. However, while an equally good fit to the GJ93 C-star LF is obtained with $\lambda = 0.6$, $\eta_{\rm AGB} = 5$, this is rejected by f(O) (Section 4.2).

The resulting PN abundances ($\lambda = 0.75$, $\eta_{\rm AGB} = 4$), as a function of initial mass and initial metallicity are shown in Fig. 1. The set of abundances summarized in Fig. 1 will be referred to as our standard model. The stellar ejecta were averaged over the last 25 000 yr, to compare with gas-phase abundances. The different PN classes based on the relative abundances of ^{12}C, ^{13}C, N and O have their niche: O-rich PNe are expected for both the lowest and highest $M_{\rm i}$ (type I PNe occurring for the highest progenitor masses), and $^{12}\mathrm{C}/^{13}\mathrm{C}$ ranges from CN equilibrium values ($\sim$3) to $>$100.

If the stellar ejecta is averaged over the last 2000 yr only, which is taken to represent warm-dust compositions (see Section 3), the contours for PN compositions are still the same as in Fig. 1 in the case of log (N/O) (albeit a noisier IIa contour). In the cases of C/O and $^{12}\mathrm{C}/^{13}\mathrm{C}$, the PN composition map as a function of ($M_{\rm i}$,$Z_{\rm i}$) is also similar to Fig. 1, but the point-to-point variations are sharper and reach higher peak values ($\sim$13 and 3000 at $t_{\rm PN} = 2000$ yr against $\sim$7 and 900 at $t_{\rm PN} = 25\,000$ yr, for C/O and $^{12}\mathrm{C}/^{13}\mathrm{C}$, respectively). There is one important change between $t_{\rm PN} = 2000$ yr and $t_{\rm PN} = 25\,000$ yr, however: in terms of the PN compositions, for $t_{\rm PN} = 2000$ yr the effects of HBB for masses higher than 4–5 $\mathrm{M}_{\odot}$ are not as dramatic, and $\mathrm{C/O} > 1$ even for the most massive progenitors (see Frost et al. 1998 for a physical discussion on the quenching of HBB).

2.2 Problems with N enrichment in PNe

In order to reproduce the range of N and C enrichment found in PNe and to account for the observed frequencies of type I and IIa PNe, we find that HBB must be much more efficient than currently modelled. As noted by Leisy & Dennefeld (1996), there is continuity in the nitrogen abundances of PNe in the LMC, with no particular grouping above the type I threshold. Yet at $Z = 0.008$, typical of the LMC, the synthetic AGB model predicts

[1] In GJ93, the density at the bottom of the convective envelope was taken as a constant 2 $\mathrm{g\,cm^{-3}}$ (Martin Groenewegen, private communication), while such a value is reached only in the most massive models of FC97.

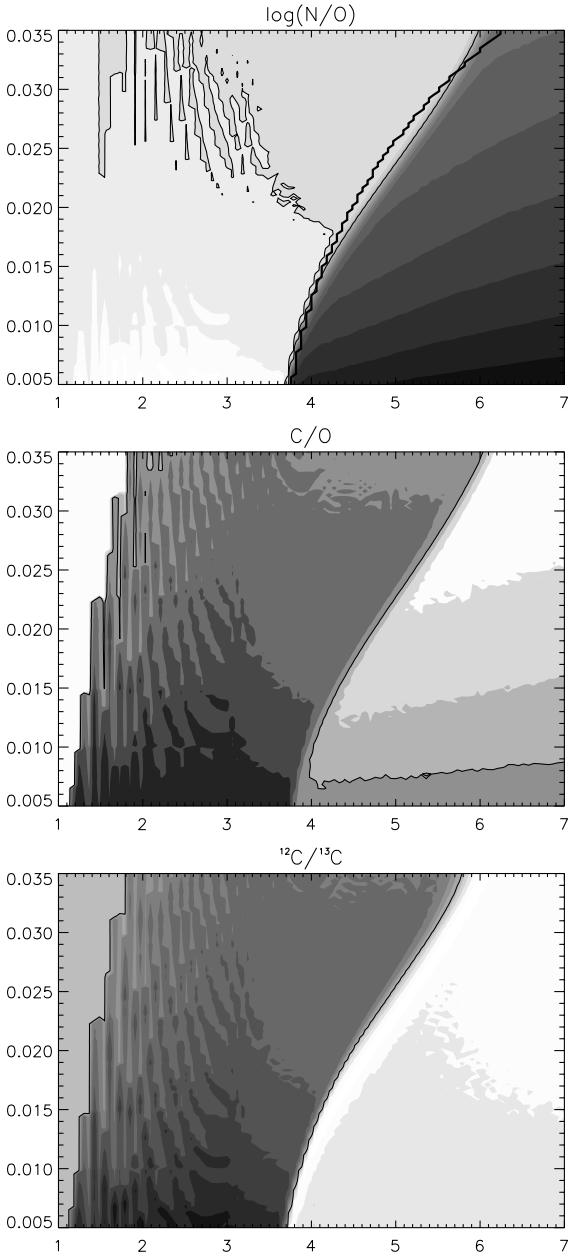

Figure 1. PN abundances averaged over the last 25 000 yr of AGB evolution as a function of initial mass in x, initial metallicity in y. From top to bottom: **log(N/O)**, with darker grey-scale contours at -0.8, -0.7, …, 0.6; the thin solid lines at -0.6 and -0.3 represent the contours for type IIa and type I PNe, while the thick line traces the minimum initial mass for the occurrence of the second dredge-up (a sharp transition at -0.3 results in missing contour levels, but the minimum and maximum plotted values of the grey-scale are -0.8 and 0.6); **C/O**, with darker contours at $\log(\mathrm{C/O}) = -0.6, \ldots, 0.4$, 0.6, and the solid line at $\mathrm{C/O} = 1$; **^{12}C/^{13}C**, with darker contours at $\log(^{12}\mathrm{C}/^{13}\mathrm{C}) = 0.7, 0.9, \ldots, 2.9$, and the solid line at $^{12}\mathrm{C}/^{13}\mathrm{C} = 30$.

no type IIa PNe at all [in the Faúndez-Abans & Maciel 1987 classification, i.e., $-0.6 < \log(\mathrm{N/O}) < -0.3$]. These conclusions also hold for the GJ93 model: with their treatment of HBB, Fig. 1 is largely unchanged (except perhaps at $Z_\mathrm{i} \sim 0.03$, where the type I threshold is at 4.6 $\mathrm{M}_\odot$ instead of 5.5 $\mathrm{M}_\odot$). Models in which core growth on the AGB is negligible, and where HBB effectively occurs above a critical core mass, predict a sharp transition in N/O ratio and progenitor mass, which is not observed.

Additionally, the majority of very C-rich PNe (those whose mid-IR spectra display the family of emission bands associated with PAHs) are of type I (Paper I). However, the existing synthetic AGB models cannot produce N-rich and very C-rich PNe in the observed frequency. Fig. 1 shows how the highest C enrichment should be found for PNe with solar N/O ratios (again, the PN composition map obtained with a 2000 yr average of AGB mass-loss leaves Fig. 1 largely unchanged). In terms of the gas-phase abundances, type I PNe are divided in their C/O chemical balance (Leisy & Dennefeld 1996, their fig. 12; see also Aller & Czyzak 1983 for Galactic disc PNe). However, the sharp onset of HBB with M_i produces O-rich PNe, exclusively (for $Z_\mathrm{i} \gtrsim 0.01$).

An exception to the above problems with synthetic AGB models is provided by RV81. It appears that RV81 underestimated the mass-loss rate ($\eta_\mathrm{AGB} \sim 1/3$ predicts excessive final masses; see GJ93, and references therein), and the extended lifetime allows the temperature at the bottom of the convective envelope to rise significantly with the growth of the core during the TP-AGB. A 3.3-$\mathrm{M}_\odot$ star can start dredging up carbon and then undergo HBB later in its evolution, in a balance that produces C- and N-rich PNe. Thus the problems with C and N enrichment in PNe could be solved by artificially fixing the slope for the increase of HBB temperature with core growth, $\mathrm{d}T_\mathrm{B}/\mathrm{d}M_\mathrm{c}$, to the values found by FC97 for their 5–6 $\mathrm{M}_\odot$ models. We found that models with $\mathrm{d}T_\mathrm{B}/\mathrm{d}M_\mathrm{c} = 2 \times 10^9\,\mathrm{K\,M_\odot^{-1}}$ produce type I and IIa PNe in the observed frequencies (around 30 and 20 per cent in the sample of Paper I; see also Maciel & Dutra 1992), with type I PNe being preferentially very C-rich. An interesting alternative to a high $\mathrm{d}T_\mathrm{B}/\mathrm{d}M_\mathrm{c}$ slope can be found in Siess & Livio (1999). The accretion of brown dwarfs or giant planets could trigger CNO processing in the convective envelope. Although the concept of envelope heating from the kinetic energy of accreted material is appealing, it is not obviously related to the observed N/O latitude effect.

Thus the N/O classification of PNe, perhaps one of their most widely used chemical characteristic, turned out to be impossible to use in PN population synthesis, at least with the models we tried. On the other hand, f(O) depends mostly on $M_\mathrm{c}^\mathrm{min}$ coupled with the core mass at the first thermal pulse (in this formalism). In fact, above a threshold initial mass, all PNe are predicted to generate C-rich warm dust during the earliest stages of their evolution. f(O) is therefore a much easier quantity to model.

2.3 Synthetic distribution of PN progenitors in the Galactic disc

A set of 10 000 stars was evolved to construct the synthetic distribution of PNe in the Galactic disc. The probability distribution for the star formation rate as a function of Galactocentric radius was extrapolated from the ultracompact H II region survey in Bronfman et al. (2000). We assumed that the number density of massive star-forming regions would also trace the number density of newly born PN progenitors. Initial stellar masses were distributed according to an initial mass function (IMF) index of -1.72 (in $\mathrm{d}N/\mathrm{d}\log M$). This index is also used in the derivation of the LMC C-star LF (Section A2.1), and is the same as in GJ93. The lower mass cut-off for the compact PNe progenitors was kept as a free parameter, M^min, and the upper mass limit was 7 $\mathrm{M}_\odot$. The IMF index may seem steep for intermediate-mass stars, and we investigated using an index of -0.95, as derived in Sabas (1997)

from a complete sample of B5–F5 stars and *Hipparcos* parallaxes (over the range 1.2–4 $M_\odot$). In this case, $M^{\rm min}$ turned out to be somewhat lower (see Section 4).

Radial diffusion in the Galactic disc was taken into account following the results presented in Köppen & Cuisinier (1997), in the epicyclic approximation. The age–velocity relation by Wielen (1977),

$$\sigma_v = \sqrt{100 + 600\frac{\rm age(M)}{10^9\,\rm yr}}\,\rm km\,s^{-1}, \quad (1)$$

in conjunction with a velocity ellipsoid of constant shape (Wielen 1977),

$$\sigma_{\rm U} : \sigma_{\rm V} : \sigma_{\rm W} = 0.79 : 0.46 : 0.41, \quad (2)$$

allows us to estimate the spread of the normal distribution by which final Galactocentric radii are distributed (Wielen, Fuchs & Dettbarn 1996),

$$\sigma_{\rm R}({\rm age}) = 1.56\sigma_{\rm U}({\rm age})/\kappa, \quad (3)$$

where $\kappa = 31.6\,\rm km\,s^{-1}\,kpc^{-1}$ is the epicyclic frequency of stellar orbits in the disc, at $R = R_0$. The factor 1.56 could altogether be neglected in this schematic treatment, which will be applied to $\approx .5 - 1.5\,R_0$.

As argued in Carraro, Yuen Keong & Portinari (1998), we adopted a radial metallicity gradient of $-0.07\,\rm dex\,kpc^{-1}$ and constant in time, and assumed a 0.005 FWHM scatter when drawing initial metallicities. $Z(R = R_0, t)$ was required to match the age–metallicity relation by Meusinger, Reimann & Stecklum (1991),

$$\begin{aligned}[\rm Fe/H](t) &\approx \log[Z(R = R_0, t)/Z_\odot] \\ &= \log[1.98 - 1.88(1 - t/28.5)^{1.25}]. \end{aligned} \quad (4)$$

3 LINKING THE MODELLED AND OBSERVED PN GALACTIC DISTRIBUTIONS

We based the comparison between modelled and observed distributions on the sample of compact and IR bright PNe from Paper I. In linking the modelled and observed PN galactic distributions, the selection effects in the PN catalogues need to be taken into account, as well as the exact relation between the AGB stellar ejecta and the observed PN compositions.

The PNe in the sample with warm dust emission were required to have *IRAS* 12-μm band fluxes in excess of 0.5 Jy. Their distribution was modelled by applying the same selection criterion to the synthetic PN population. It is shown in Paper I that the PNe with warm dust should be optically thick in the Lyman continuum, in which case the four *IRAS* bands give a good representation of their bolometric flux, with a fraction of 0.25 ± 0.14 of the total flux in the 12-μm band. The IR-bright selection criterion should probe the whole of the Galactic disc. However, selection effects that limit the Galactic disc sampling area come from the optical discovery surveys. Extinction in the Galactic disc needs to be taken into account. Condon & Kaplan (1998) report extinction values towards 429 PNe; no PNe are found with $c = \log(\rm H\beta^{real}/H\beta^{obs})$ in excess of 3.3, with an approximate cut-off in the distribution at $c \sim 2$. They also show that c depends strongly on galactic coordinates, with values of order 1 towards the Galactic anticentre. The bulk of the extinction to PNe is thus Galactic, rather than intrinsic, and a maximum value of $c = 2$–3.5 would give $A_V = 3.8 - 6.6$. We adopted a maximum interstellar extinction of $A_V = 4$, as for the objects with warm dust intrinsic extinctions of at least one magnitude have been reported.

A Gaussian profile[2] in Galactocentric radius for $\Lambda(R)$, the 'linear density of extinction', gives

$$A_V({\rm D,l}) = \int_0^D {\rm d}s\,\Lambda(R) = \int_0^D {\rm d}s\,A\exp\left(-\frac{R^2}{2R_{\rm A}^2}\right). \quad (5)$$

The values of $A = 4\,\rm mag\,kpc^{-1}$ and $R_{\rm A} = 3.6\,\rm kpc$ were fixed by requiring $A_{\rm GC} = 20\,\rm mag$ for the extinction to the Galactic Centre, and a minimum Galactocentric radius of $0.5\,R_0$ for $A_V^{\rm max} = 4$. These requirements give a local linear density of visual extinction of only $0.25\,\rm mag\,kpc^{-1}$, and the value of $A_{\rm GC} = 20\,\rm mag$ may seem low as well. However, we did not take into account the dependence of $\Lambda(R)$ on height above the Galactic plane, and the fact that PNe would preferentially be discovered towards directions of low extinction: if the average linear density of extinction to local PNe were really $1\,\rm mag\,kpc^{-1}$, no PNe would be detected beyond 4 kpc. It is apparent from fig. 6 in Paper I that the maximum distance to Galactic disc PNe with warm dust is about 8 kpc, which we adopted as a maximum distance in the synthetic population. This estimate of the sampled area in the Galactic disc is intended to approximate the observed face-on distribution.

In the case of the PNe with warm dust emission features, the problem of a lifetime dependence on the progenitor mass is greatly simplified by the presumed youth of the objects. We assumed that the compact and IR-bright PNe with warm dust emission all have the same lifetime, neglecting any dependence on $M_{\rm i}$. However, it should be kept in mind that the durations of the 'warm-dust' phase lifetimes could depend on the dust opacities. It was suggested to us (Kevin Volk, private communication) that this could be the reason why the fraction of O-rich objects is $f({\rm O}) \sim 22$ per cent from the dust grain compositions, while it is closer to 40 per cent from the plasma diagnostics. Some arguments against this possibility may be found in section 6 of Paper I, and the next section develops the idea that the difference in $f({\rm O})$ could be due to the different time-scale over which the AGB ejecta should be averaged ($t_{\rm PN}$ in this work). In any case, the conclusions we reach on $f({\rm O})$ being a tight constraint on AGB parameters are valid even if $f({\rm O}) \sim 50$ per cent.

A lower metallicity limit for the production of dust is discarded, as even some very low-metallicity PNe show warm-dust emission (e.g., in a forthcoming paper on bulge PNe, we will report on the type IV PN M 2-29, which shows the silicate signature in spite of a very low O abundance of $[{\rm O/H}] = -1.4\,\rm dex$, as estimated by Ratag et al. 1997).

Since PNe with no warm dust correspond to later evolutionary stages (Paper I), the link between the computed C/O ratios and the dust features is very tight. As discussed in Paper I, silicates represent ${\rm C/O} < 1$, and SiC and UIR bands ${\rm C/O} > 1$. The only problem left in linking the synthetic and observed PN populations is defining how to compute the average compositions. If the warm dust grains are heated directly by radiation from the central stars, then a temperature of 100–200 K places the grains at $\sim 10^{16}$ cm from the exciting star, which corresponds to an ejection age of

[2] Köppen & Vergeley (1998) modelled the Galactic disc extinction by matching an exponential linear density of extinction in R and z to bulge PNe. However, the dust and molecular content at $R \lesssim 2$ is similar to that of the molecular ring at $R \sim 0.5\,\rm R_\odot$ (Bronfman et al. 1988; Deul & Burton 1991), and it is not clear whether there is a sharp central concentration of dust in the Galactic disc.

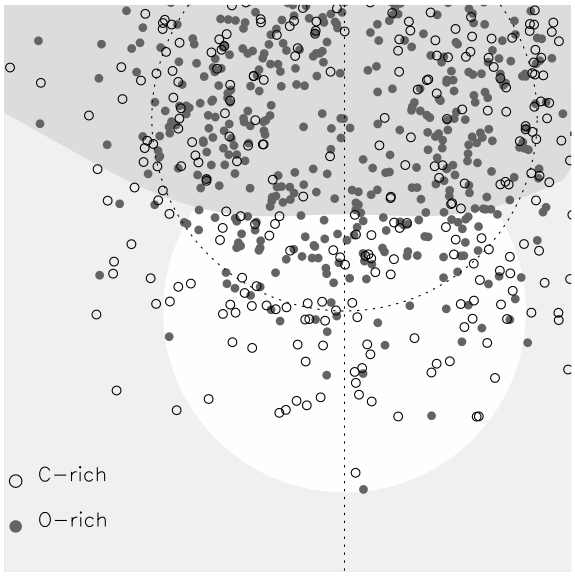

Figure 2. Synthetic distribution of PNe in the Galactic disc, with filled circles representing O-rich nebulae, and open circles C-rich nebulae. The dotted lines correspond to the solar circle ($R_0 = 8.5$ kpc) and to $l = 0$. The clear area is the region where sources would have been included in the PN catalogues, within the adopted limit of $A_V = 4$ and $d_{\max} = 8$ kpc. The AGB mass-loss was averaged over the last 2000 yr of evolution. For the clarity of the plot, the initial number of PNe is only 1000, and comes down to ~200 within the Galactic disc sampling area. This figure can be compared to fig. 6 in Paper I.

400 yr at $10\,\mathrm{km\,s^{-1}}$. In this picture, the warm dust grain composition derives from the very last stages of AGB evolution. Thus the PNe compositions were averaged over the last 2000 yr, to compare with the dust emission features, while a more typical 25 000 yr was used to compare with the gas-phase abundances.

The resulting synthetic distribution can be seen in Fig. 2, in the case of a minimum progenitor mass of $1.2\,\mathrm{M}_\odot$. Galactocentric azimuths were drawn from a uniform random distribution.

4 RESULTS: THE MINIMUM MASS FOR PN PROGENITORS

4.1 The minimum mass for PN progenitors

Having calibrated all the free parameters in the synthetic AGB model, the mass range for PN progenitors still needs to be specified. The lower mass limit has a direct influence on the synthesized PN distribution, although the exact upper mass limit is of secondary importance, high-mass stars being less frequent.

The property of the synthetic distribution that can be most directly compared to the observed distribution of PNe with warm dust is the relative frequency of C- and O-rich nebulae. Shown in Fig. 3 is the fraction of O-rich PNe as a function of minimum progenitor mass, $M^{\min}$, for the set of parameters given in Section 2.1. PN compositions were computed by averaging the stellar mass-loss over the last $t_{\rm PN} = 2000$ yr of evolution on the AGB to compare with the dust signatures. The shaded areas correspond to the range of observed values within $\pm 1\sigma$ (from Paper I),

$$f(\mathrm{O\ rich}) = 0.22 \pm 0.06. \quad (6)$$

In order to match the observations, $M^{\min}$ is constrained to

$$M^{\min} > 1.2\,\mathrm{M}_\odot \quad (7)$$

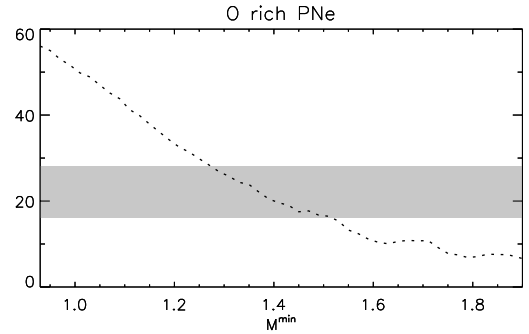

Figure 3. The fraction of O-rich PNe, f(O), as a function of minimum main-sequence progenitor mass, $M^{\min}$. The shaded area corresponds to the observed values within 1σ.

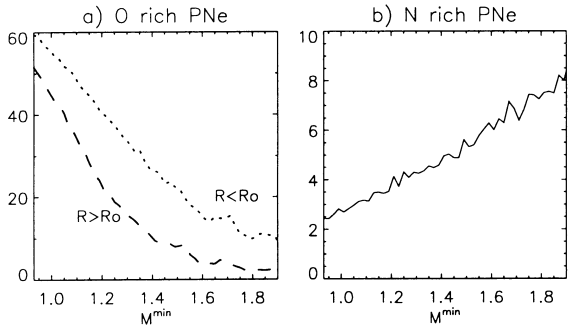

Figure 4. Properties of the synthetic PN population as a function of minimum main-sequence progenitor mass, $M^{\min}$. (a) f(O) inside and outside the solar circle, (b) the fraction of type I PNe (the observed values is 29 ± 6 per cent, from Paper I and references therein).

at 2σ confidence level (or $\sim 1.3\,\mathrm{M}_\odot$ at 1σ). The IMF slope in our standard model is rather steep, and for comparison a shallow IMF of index −0.95 (Sabas 1997) gives $M^{\min} > 1.2\,\mathrm{M}_\odot$ at 1σ; f(O) does not seem to be very sensitive on the IMF.

We will now test the value of $M^{\min}$ against less accurate properties of the observed PN distribution, and analyse trends with Galactocentric radius. In the synthetic PN distribution, the relative number of PNe inside and outside the solar circle is $N_{\rm in}/\mathrm{N}_{\rm out} = 1.3$ (rather independent of $M^{\min}$), while the observed ratio is 0.9–1.6 (from tables 6 and 7 in Paper I), depending on the PN distance scale. The approximate agreement is an indication that the Galactic disc sampling area of Section 3 is appropriately defined.

Fig. 4(a) shows the fraction of O-rich PNe, f(O), for $R < R_0$ and $R > R_0$. There is a clear decrease in the model f(O), for any value of $M^{\min}$, and it is thus a robust property of the synthetic distribution. From Paper I, the observed f(O) is 30 ± 9 per cent inside the solar circle, and 14 ± 7 per cent outside. Fig. 4(b) shows the proportion of type I PNe as a function of minimum progenitor mass. For any $M^{\min}$, the fraction of type I PNe is far too low. This result can also be reached by estimating the proportion of progenitors between $M^{\min}$ and $\sim 4\,\mathrm{M}_\odot$, even for a shallow IMF. Either this is yet another deficiency of current models for N enrichment, or the PN sample is dramatically affected by biases against low-mass progenitors. The latter case seems rather contrived; a complete PN sample is a working hypotheses for this paper, and in the event of a strongly biased sample, $M^{\min}$ represents a lower mass limit above which we trust the observed f(O) – as well as f(type I). Additionally, we know that N enrichment is not satisfactorily modelled (e.g. Section 2.2).

For comparison the gas-phase abundance distribution synthesized with $t_{\rm PN} = 25\,000$ yr predicts 5–12 per cent more O-rich PNe, depending on $M^{\rm min}$, and around 28 per cent for $M^{\rm min} = 1.4\,{\rm M}_\odot$ [which gives $f({\rm O}) = 22$ per cent if $t_{\rm PN} = 2000$]. This is due to a contribution of O-rich objects produced by HBB, which is quenched over the last 2000 yr. In the sample of Paper I, this fraction is 40 ± 8 per cent, and is ∼40 per cent in Zuckerman & Aller (1986; note that their sample is inhomogeneous, with a broad range of PN ages). The gas-phase C/O ratio is available for an even more restricted number of sources (of the ones with warm dust), and is subject to large uncertainties stemming from the difficulties in measuring the C abundance, especially in compact and IR-bright PNe – compare for instance Aller & Czyzak (1983) and Henry et al. (2000), in the cases of NGC 3242 and 6826. Considering such uncertainties, we believe that the difference between the fraction of O-rich PNe, as inferred from the dust compositions and the plasma diagnostics, is due to $t_{\rm PN}$.

In the framework of an artificially high ${\rm d}T_{\rm B}/{\rm d}M_{\rm c}$ (Section 2.2), the effects of $t_{\rm PN}$ on $f({\rm O})$ are stronger because HBB occurs for lower progenitor masses and is thus more frequent. Accounting for the observed proportions of type I and IIa PNe (29 ± 6 per cent and 12 ± 6 per cent; Paper I) would give an upper limit to $M^{\rm min}$ of about $1.4\,{\rm M}_\odot$ (above this limit, there are too many type I PNe). With $M^{\rm min} = 1.2\,{\rm M}_\odot$ and $t_{\rm PN} = 2000$ yr, the fraction of C-rich PNe that have Peimbert type I is 35 per cent, and the observed proportion of type I PNe among PNe with C-rich dust grains is 37 ± 10 per cent (Paper I). Similarly, in the synthetic distribution the fraction of O-rich PNe that have Peimbert type I is 26 per cent, and the observed proportion of type I PNe among those with O-rich dust is 22 ± 14 per cent.

4.2 Model sensitivity

What is the model sensitivity of the predicted fraction of O-rich PNe? Of the relations used in the synthetic AGB model, which are the ones responsible for the Galactic gradient in $f({\rm O})$, i.e., which are the most sensitive to the Galactic metallicity gradient?

The predicted fraction of O-rich PNe is a sensitive function of the free parameters, as shown in Fig. 5(a). The sets of parameters correspond to a range of third dredge-up efficiencies, over an AGB star's lifetime (an extended lifetime results in more dredge-up episodes). However, at first sight of Figs 5(b) and (c), all models seem to reproduce acceptably the C-star LF used in GJ93 or that from CF96 (with 1σ uncertainties of ∼10 per cent at the peak). In terms of the C-star LF χ^2 values, which we calculated summing over each logarithmic luminosity bin, from 4 to 5.8 for the CF96 LF and from 4.125 to 5.625 for the GJ93 LF, the AGB parameters adopted by GJ93 ($\eta_{\rm AGB} = 4$ and $\lambda = 0.75$) seem reasonable. We assumed the GJ93 LF was built with 298 sources, about 3 times less than in CF96 (895 sources). However, the associated χ^2 confidence levels are very low (with 7 and 10 degrees of freedom for GJ93 and CF96, respectively). It is difficult to assess the quality of the C-star LF fit, from one set of parameters to another. It turns out the C-star LF χ^2 values are very noisy: for the set of AGB parameters $(\lambda, \eta_{\rm AGB}) = \{(1,1),\ (0.9,2),\ (0.9,3),\ (0.6,3),$

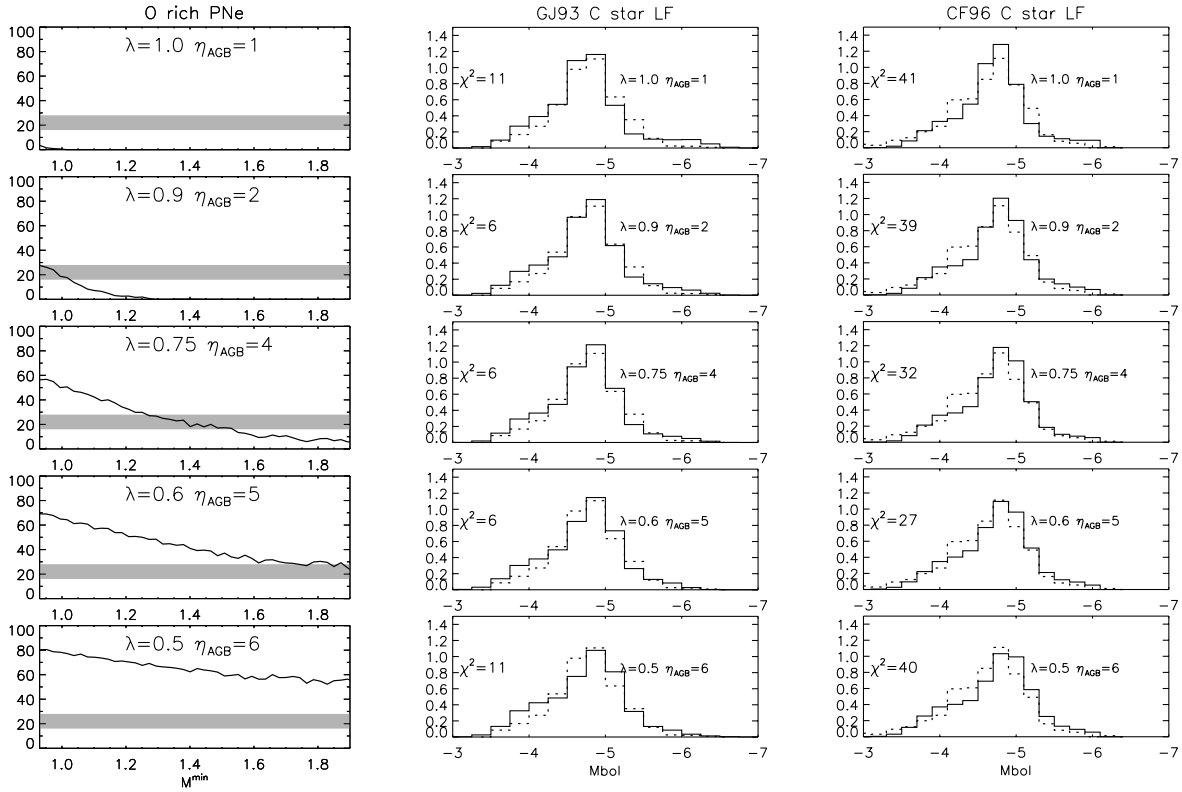

Figure 5. (a) The fraction of O-rich PNe in the solar neighbourhood, in solid lines, are model results from PN population synthesis as a function of minimum progenitor mass (in $\rm M_\odot$). The shaded area corresponds to the observed fraction $\pm 1\sigma$. $\eta_{\rm AGB}$ is the mass-loss coefficient of a scalable Reimers law, and λ is the third dredge-up parameter. (b) Synthesis (solid line) of the LMC C-star LF used in GJ93 (dotted line), for the same sets of parameters as in (a). (c) Synthesis (solid line) of the observed (dotted line) LMC C-star LF from CF96.

(0.75,4), (0.6,4), (0.75,5), (0.6,5), (0.5,6)}, $\chi^2 = (11, 6, 14, 7, 6, 8, 10, 6, 11)$ for the GJ93 LF, and $\chi^2 = (41, 39, 24, 56, 32, 39, 28, 27, 40)$ for the CF96 LF. On the other hand, f(O) exhibits broad variations over the same set of AGB parameters, and the last two models with $\eta_{\rm AGB} = 5$ are clearly rejected. Models with $\eta_{\rm AGB} = 2$ and $\lambda < 0.6$ predict excessive final masses (see Section A2.2), and $M^{\rm min} \lesssim 1$ is unlikely considering the extremely low proportion of type I PNe (around 3 per cent). We stress that the constraints put on the AGB parameters are model-dependent; rejected parameters could well fit another set of AGB prescriptions. Our purpose here is to illustrate the usefulness of PN population synthesis, provided a proper PN sample is built.

Of the relations used in the synthetic AGB model (see Appendix A), the following include an explicit metallicity dependence:

(1) core-mass versus interpulse period relation;
(2) mass-loss prior to the AGB;
(3) core-mass at the first thermal pulse;
(4) luminosity at the first thermal pulse;
(5) core-mass versus luminosity relation;
(6) $T_{\rm eff}(L, Z, M)$;
(7) evolution rate, and
(8) hot bottom burning density and temperature.

The synthetic PN population was tested for sensitivity to the Galactic metallicity gradient by fixing the metallicity entry of all the previously listed relations at $Z = 0.02$. The initial composition was kept as described in Appendix A, i.e., a metallicity-scaled solar mix, with a Galactic metallicity gradient and an age–metallicity relation. The resulting synthetic PN population did not show a gradient in the fraction of O-rich PNe. Subsequently the constraint on the metallicity was relaxed one relation at a time, and the resulting model population was inspected using the equivalent of Fig. 4(a). The difference in the fraction of O-rich PNe inside and outside the solar circle was used to test the dependence upon the metallicity gradient.

The most sensitive relations are $T_{\rm eff}(L, Z, M)$ and the core-mass at the first thermal pulse. The other relations resulted in an insignificant change in the fraction of O-rich PNe inside and outside R_0. The synthetic population generated using a flat metallicity profile was confirmed not to show a gradient in the fraction of O-rich PNe. The metallicity dependence of f(O) resides in the following.

(i) $T_{\rm eff}$ increases with lower metallicity, which for a fixed luminosity translates into a lower envelope radius, and a lower mass-loss rate. The extended AGB-lifetime thus leaves more time for core growth and the C-enrichment of the envelope. The relation used here for $T_{\rm eff}$, is a model result from Wood (1990; see also Vassiliadis & Wood 1993).

(ii) The core-mass at the first thermal pulse, $M_{\rm c}(1)$, is a decreasing function of metallicity. Together with a fixed minimum core-mass for the occurrence of the third dredge-up (the free parameter $M_{\rm c}^{\rm min}$), the lower limit progenitor ZAMS mass for the production of C-rich nebulae decreases with metallicity.

A full search in all possible combinations in parameter space is postponed to a future investigation, based on a more solid AGB model, and a larger PN sample.

5 CONCLUSIONS

PN population synthesis was investigated using a schematic model for AGB evolution, whose free parameters were calibrated with the luminosity function of C stars in the LMC and the initial–final mass relation. The Galactic distribution of PN progenitors was generated using the observed metallicity gradient and distribution of star-forming regions with Galactocentric radius. The PNe with warm dust emission from Paper I represent a homogeneous population, which is presumably young and thus minimally affected by a possible dependence of PN lifetime on progenitor mass. We examined the consequences of assuming the statistics of PN compositions in the sample of Paper I reflect tip-of-the-AGB values, and reached the following conclusions.

(i) The fraction of PNe with O-rich dust places constraints on the range of PN progenitor masses. A minimum PN progenitor mass of $1\,{\rm M}_{\odot}$ predicts that about 50 per cent of all young PNe should be O-rich, whereas only 22 per cent are observed. The minimum PN progenitor mass required to reproduce the properties of the observed distribution of PNe with warm dust is $M^{\rm min} = 1.2$, at a 2σ confidence level.

(ii) The observed decrease in the fraction of O-rich PNe with Galactocentric radius is a robust property of the synthetic distribution.

(iii) Independently of $M^{\rm min}$, values for the dredge-up parameter λ and the mass-loss rate parameter $\eta_{\rm AGB}$ that reproduce the LMC C-star LF do not necessarily match the observed fraction of O-rich PNe, f(O).

The relative frequencies of C- and O-rich PNe depend mostly on the value of the minimum core mass for C dredge-up, which is calibrated with the LMC C-star LF (as in GJ93). However, the treatment of HBB is of crucial importance in predicting PN compositions, as it directly accounts for the Peimbert (1978) types. Measurements of the ^{12}C to ^{13}C isotopic ratio in PNe can provide an observational test, since a transition from >100 to ~ 3 is expected with the onset of HBB (e.g. RV81).

Overall, the good agreement obtained with the observed PN distribution is an indication that the statistics of dust signatures in PNe can be used as probes of their progenitor population in various Galactic environments.

ACKNOWLEDGMENTS

We are grateful to Mike Barlow, Robin Clegg, Edgardo Costa and Philipp Podsiadlowski for interesting feedback and encouraging discussions. SC acknowledges support from Fundación Andes and PPARC through a Gemini studentship.

REFERENCES

Aller L. H., Czyzak S. J., 1983, ApJS, 51, 211
Barlow M. J., 1983, in Flower D. R., ed., Proc. IAU Symp. 103, Planetary Nebulae. Reidel, Dordrecht, p. 105
Blanco V. M., McCarthy M. F., 1983, AJ, 88, 1442
Boothroyd A. I., Sackman I. J., 1988, ApJ, 328, 653
Bronfman L., Cohen R. S., Alvarez H., May J., Thaddeus P., 1988, ApJ, 324, 248
Bronfman L., Casassus S., May J., Nyman L. A., 2000, A&A, 358, 521
Bryan G. L., Volk K., Kwok S., 1990, ApJ, 365, 301
Carraro G., Yuen Keong N., Portinari L., 1998, MNRAS, 296, 1045
Casassus S., Roche P. F., Aitken D. K., Smith C. H., 2001, MNRAS, 320, 424 (Paper I, this issue)
Caughlan G. R., Fowler W. A., 1988, Atomic Data and Nuclear Data Tables, 40, 2

Clayton D. D., 1968, Principles of Stellar Evolution and Nucleosynthesis. McGraw-Hill, New York
Condon J. J., Kaplan D. L., 1998, ApJS, 117, 361
Costa E., Frogel J. A., 1996, AJ, 112, 2607 (CF96)
Deul E. R., Burton W. B., 1991, The Galactic Interstellar Medium, Saas Fée Advanced Course 21, p. 79
Faúndez-Abans M., Maciel W. J., 1987, A&A, 183, 324
Forestini M., Charbonnel C., 1997, A&AS, 123, 241 (FC97)
Frost C. A., Cannon R. C., Lattanzio J. C., Wood P. R., Forestini M., 1998, A&A, 332, L17
Groenewegen M. A. T., de Jong T., 1993, A&A, 267, 410 (GJ93)
Groenewegen M. A. T., van den Hoek L. B., de Jong T., 1995, A&A, 293, 381
Henry R. B. C., Kwitter K. B., Bates J. A., 2000, ApJ, 531, 928
Hughes S. M. G., 1989, AJ, 97, 1634
Hughes S. M. G., Wood P. R., 1990, AJ, 99, 784
Iben I., Jr, 1985, QJRAS, 26, 1
Iben I., Jr, Laughlin G., 1989, ApJ, 341, 312
Iben I., Jr, Truran J. W., 1978, ApJ, 224, L63
Jura M., Joyce R. R., Kleinmann S. G., 1989, ApJ, 336, 924
Kaler J. B., Iben I., Jr, Becker S. A., 1978, ApJ, 224, L63
Köppen J., Cuisinier F., 1997, A&A, 319, 98
Köppen J., Vergeley J.-L., 1998, MNRAS, 299, 567
Lattanzio J. C., 1989, ApJ, 347, 989
Leisy P., Dennefeld M., 1996, A&AS, 116, 95
Maciel W. J., Dutra C. M., 1992, A&A, 262, 271
Marigo P., Bressan A., Chiosi C., 1996, A&A, 313, 545
Marigo P., Girardi L., Bressan A., 1999, A&A, 344, 123
Meusinger H., Reimann H.-G., Stecklum B., 1991, A&A, 245, 57
Peimbert M., 1978, in Terzian Y., ed., Proc. IAU Symp. 76, Planetary Nebulae. Reidel, Dordrecht, p. 233
Podsiadlowski P., 1989, PhD thesisM.I.T.,
Ratag M. A., Pottash S. R., Dennefeld M., Menzies J., 1997, A&AS, 126, 297
Reimers D., 1975, in Basheck B. et al., eds, Problems in Stellar Atmospheres and Envelopes. Springer, Berlin, p. 229
Renzini A., Voli M., 1981, A&A, 94, 175 (RV81)
Roche P. F., 1989, in Torres Peimbert S., eds, Proc. IAU Symp. 131, Planetary Nebulae. Kluwer, Dordrecht, p. 117
Sabas V., 1997, Proceedings of the ESA Symposium 'Hipparcos-Venice '97', ESA SP-402, 563
Siess L., Livio M., 1999, MNRAS, 304, 925
Smith V. V., Lambert D. L., 1986, ApJ, 311, 843
Thronson H. A., Latter W. B., Black J. H., Bally J., Hacking P., 1987, ApJ, 322, 770
Trams N. R. et al., 1999, A&A, 344, L17
van Loon J. Th., Zijlstra A. A., Groenewegen M. A. T., 1999, A&A, 346, 805
Vassiliadis E., Wood P. R., 1993, ApJ, 413, 641
Wagenhuber J., Groenewegen M. A. T., 1998, A&A, 340, 183
Weidemann V., 1987, A&A, 188, 74
Weidemann V., Koester D., 1983, A&A, 121, 77
Wielen R., 1977, A&A, 60, 263
Wielen R., Fuchs B., Dettbarn C., 1996, A&A, 314, 438
Wood P. R., 1990, in Mennessier M. O., Omont A., eds, From Miras to Planetary Nebulae. Editions Frontières, Gif-sur-Yvette, p. 67
Zuckerman B., Aller L. H., 1986, ApJ, 301, 772

APPENDIX A: ANALYTICAL PRESCRIPTIONS FOR AGB EVOLUTION AND CALIBRATION OF FREE PARAMETERS

A1 Synthetic AGB evolution code

To summarize, we will describe the steps followed in the code, for a star with fixed (M_i, Z_i). All the analytical prescriptions are written in GJ93, except when explicitly indicated as not being so. The initial composition is calculated assuming the relative abundances of the elements are the same as in the solar mix. We follow the steps in GJ93 up to the first thermal pulse, taking the mass-loss prescription on the E-AGB from Groenewegen et al. (1995, their equation 1). The core mass and luminosity at the first thermal pulse, $M_c(1)$ and $L(1)$, are the initial conditions for the TP-AGB. $M_c(1)$ is of significant importance, since it fixes for the most part the initial–final mass relation, one of the observational constraints. GJ93 take $M_c(1)$ from Lattanzio (1989) for M_i under $3\,M_\odot$, and from RV81 above. The subsequent TP-AGB evolution is described by a loop, in which the interpulse period t_{ip} is determined by a core-mass versus interpulse relation (from Boothroyd & Sackmann 1988; GJ93 include a 'turn-on' phase). The luminosity is given by a core-mass versus luminosity relation, with the fits in GJ93 (Iben & Truran 1978; Boothroyd & Sackmann 1988), who use a rectangular profile to account for the luminosity dip and flash. GJ93 calculate the rate of core growth from the luminosity due to hydrogen burning.[3] The mass-loss rate is estimated via a $\boldsymbol{\eta}_{AGB}$ scalable Reimers (1975) law. The stellar radius R is estimated from the (model) relation given by Wood (1990) between the luminosity and the effective temperature of O-rich Miras. The condition for ending the AGB is then tested (based on a critical envelope mass; Iben 1985), as well as the end of the interpulse period. In the case of a new thermal pulse, the condition for dredge-up is tested: $M_c > M_c^{min}$. M_c^{min} is one of the free parameters in GJ93.

The process following a third dredge-up event is the most sensitive part of this code, and it affects the PN compositions directly. It is standard to model the dredged-up material enriched in He and ^{12}C as a fraction $\boldsymbol{\lambda} \sim 0.6$ of the core growth during the interpulse period ΔM_c,

$$\Delta M_{dredged} = \lambda\, \Delta M_c. \qquad \text{(A1)}$$

λ could well be a function of metallicity or other parameters, but is here taken as a constant. The composition of the dredged-up material, the result of incomplete helium burning, is taken from Boothroyd & Sackmann (1988), $Y^{3rd-du} = 0.76$, $^{12}C^{3rd-du} = 0.22$, $^{16}O^{3rd-du} = 0.02$. In the absence of HBB, the dredged-up material is simply diluted in the envelope.

HBB is the main source of uncertainties in the model: existing AGB models for single stars have difficulties in producing N- and C-rich PNe (see Section (sec:pb_N). HBB was treated by setting the initial temperature $T_B(1)$ and density $\rho_B(1)$ at the bottom of the convective envelope to the values listed in FC97. We first interpolated in $\log T_B(1)$ and $\log \rho_B(1)$ as functions of $M_c(1)$, for the two metallicity cases listed (LMC and solar), and then in $\log T_B(1)$ and $\log \rho_B(1)$ as functions of metallicity Z. For the subsequent evolution on the TP-AGB, we used the model results in FC97 as a function of time to estimate dT_B/dM_c and $d\rho_B/dM_c$. They obtained constant growth rates for ρ_B and T_B, and we assumed core growth to be roughly linear in time (as it is in GJ93), and given by table 5 in FC97. A more accurate treatment is pointless, as major adjustments to dT_B/dM_c are required to explain the observations. Thus the results in FC97 led us to the following prescriptions for $d\rho_B/dM_c$ and dT_B/dM_c, with upper limits

[3] We did not include a luminosity increment due to HBB. The observational constraint is the C-star LF, and a HBB correction would affect only massive M giants (and their mass-loss rate), which go in the C-phase at the very end of the AGB; see Fig. A1.

$\mathrm{d}\rho_\mathrm{B}/\mathrm{d}M_\mathrm{c} < 10^3\,\mathrm{g\,cm^{-3}\,M_\odot^{-1}}$, $T_\mathrm{B} < 10^8\,\mathrm{K}$, $\rho_\mathrm{B} < 1$:

$$\log\frac{\mathrm{d}T_\mathrm{B}}{\mathrm{d}M_\mathrm{c}} = \begin{cases} 8.33M_\mathrm{c}(1) + 2.05, & Z = 0.02, \\ 6.85M_\mathrm{c}(1) + 3.51, & Z = 0.008, \end{cases} \tag{A2}$$

$$\log\frac{\mathrm{d}\rho_\mathrm{B}}{\mathrm{d}M_\mathrm{c}} = \begin{cases} 14.3M_\mathrm{c}(1) - 10.4, & Z = 0.02, \\ 13.1M_\mathrm{c}(1) - 9.23, & Z = 0.008. \end{cases} \tag{A3}$$

As explained in Section 2.2, a significant increase in T_B during the AGB is required to explain C- and N-rich PNe. Equation (A2) does not provide such a strong increase, except for the highest masses. As many uncertainties affect the treatment of HBB anyway, we investigated treating $\mathrm{d}T_\mathrm{B}/\mathrm{d}M_\mathrm{c}$ as a free parameter, and satisfactory results are obtained for $\mathrm{d}T_\mathrm{B}/\mathrm{d}M_\mathrm{c} = 2\times10^9\,\mathrm{K\,M_\odot^{-1}}$.

Once T_B and ρ_B are determined, dredged-up material is exposed to CNO processing over a time t_HBB, and material in the envelope is processed during $t_\mathrm{HBB}\ \mathrm{t_{ip}}/\tau_\mathrm{conv}$, where $\tau_\mathrm{conv} \sim 0.5\,\mathrm{yr}$ is the convective turn-over time-scale[4] (as quoted in FC97). We fixed $t_\mathrm{HBB} = 10^{-6}\,\mathrm{yr}$ so as to obtain $^{12}\mathrm{C}/^{13}\mathrm{C}$ ratios at CN equilibrium values for the most massive stars, while avoiding the onset of the full tri-cycle (which is not reported to occur in the envelope of AGB stars, and reduces the O abundances to produce C/O ratios of order 10). In the HBB treatment of GJ93, the envelope cannot reach $^{12}\mathrm{C}/^{13}\mathrm{C}$ at equilibrium values, since they took only a very small fraction ($\sim10^{-4}$) of the envelope mass to be CNO-processed. In GJ93 dredge-up material is fully exposed, with $^{12}\mathrm{C}/^{13}\mathrm{C} \sim 3$, but it is C-deficient, and $^{13}\mathrm{C}$ is diluted in the envelope. It is worth noting that even with these differences for HBB, the equivalent of Fig. 1 for the model in GJ93 HBB is identical – except for $^{12}\mathrm{C}/^{13}\mathrm{C}$. The injection of triple-alpha enriched material in the envelope is given by

$$\Delta Y^\mathrm{du} = Y^\mathrm{3rd-du}\,\Delta M_\mathrm{dredged}, \tag{A4}$$

$$\Delta X_i^\mathrm{du} = \frac{1}{t_\mathrm{HBB}}\int_0^{t_\mathrm{HBB}} X_i(t)\,\mathrm{d}t\Delta M_\mathrm{dredged}, \tag{A5}$$

with initial conditions for the abundance of element i, $X_i(0)$ given as above, or otherwise taken as zero. The change in the surface abundances is

$$X_i^\mathrm{new} = \frac{\Delta\mathrm{X_i^{du}} + \dfrac{\mathrm{M_{env}}}{\mathrm{t_{HBB}^{env}}}\displaystyle\int_0^{\mathrm{t_{HBB}^{env}}}\mathrm{X_i(t)\,dt}}{\mathrm{M_{env}} + \Delta\mathrm{M_{dredged}}}, \tag{A6}$$

where $t_\mathrm{HBB}^\mathrm{env} = \mathrm{t_{HBB}t_{ip}}/\tau_\mathrm{conv}$, and the initial condition for the time average of CNO processing is taken as $X_i(0) = X^\mathrm{old}$. The nuclear reaction rates for the CNO tri-cycle were taken from Caughlan & Fowler (1988), and we followed the analytical treatment in Clayton (1968), with approximations for the branching ratios between the main CN-cycle and the two secondary cycles from Podsiadlowski (1989).

As explained in Frost et al. (1998), there is a minimum envelope mass below which HBB is quenched. The critical envelope mass $M_\mathrm{HBB}^\mathrm{env}$ was adapted from GJ93,

$$M_\mathrm{HBB}^\mathrm{env} = 0.85\,\mathrm{M_{pn}}, \tag{A7}$$

$$M_\mathrm{pn} = b(1.687 - 9.092\,M_\mathrm{c} + 11.687\,M_\mathrm{c}^2 - 4.343\,M_\mathrm{c}^3), \tag{A8}$$

where M_pn is the RV81 criterion for PN ejection with $b = 0.5$. The exact value of b and the 0.85 factor are of secondary importance, GJ93 having fixed these parameters to match the results in RV81.

We stress here that dredge-up must occur after HBB is quenched. Observational support can be found in Trams et al. (1999) and van Loon, Zijlstra & Groenewegen (1999). It is of crucial importance for explaining the vast majority of N-rich PNe with C-rich dust (corresponding approximately to the last 2000 yr of AGB mass-loss).

[4] The value of τ_conv is of secondary importance. The total exposure time is $t_\mathrm{HBB}\ \mathrm{t_{ip}}/\tau_\mathrm{conv}$, and any change in τ_conv can be compensated with t_HBB.

A2 Observational constraints

A2.1 The luminosity function of C stars in the LMC

The population of stars in the LMC with initial masses between M and $M + \mathrm{d}M$ which are currently on the TP-AGB is

$$N(M)\,\mathrm{d}M \propto \mathrm{SFR(M)} \times \mathrm{IMF(M)} \times \mathrm{t_{AGB}(M)}\,\mathrm{d}M, \tag{A9}$$

where SFR(M) is the star formation rate in the LMC at time $t(M)$, the time of birth as a function of mass, IMF(M) is the initial mass function, which will be taken as a power law, and t_AGB(M) is the lifetime on the TP-AGB as a function of main-sequence mass. There is an implicit metallicity dependence via the LMC age–metallicity relation. In practice, we started with $N(M)\,\mathrm{d}M \propto \mathrm{SFR(M)} \times \mathrm{IMF(M)}$, and weighted the result with t_AGB(M). The procedure is equivalent to multiplying each mass entry by t_AGB(M) (times an integer big enough to keep a satisfactory resolution).

The parameters describing the global evolution of the LMC were reproduced from GJ93. The star formation rate in the LMC is approximated as $\mathrm{SFR(M)} \propto \exp[-\mathrm{t(M)}/7]$; with $t(M)$ in Gyr and an LMC age of $\tau_\mathrm{LMC} = 11\,\mathrm{Gyr}$, the initial mass function is $\mathrm{IMF(M)} \propto \mathrm{M}^{-2.72}$, and the age–metallicity relation is assumed to be linear in time, $Z(t) = 0.01 - 0.008 \times (1 - t/13)$. The total lifetime as a function of mass, $t(M)$, was taken from Iben & Laughlin (1989).

Observational data with which to constrain the AGB population in the LMC is compiled in GJ93. The luminosity function of C stars is a very good constraint, since there can be no doubt on their evolutionary status (i.e., at the luminosity implied by the LMC distance, C stars can only be on the TP-AGB). On the other hand, the relative frequency of C and M stars is much more uncertain: the contamination from M stars on the E-AGB is difficult to estimate. Hughes (1989) and Hughes & Wood (1990) found that most LPVs in the LMC have spectral type M5+, and $\mathrm{C/M} = 0.63$, provided that all M stars on the TP-AGB are also LPVs. Based on previous measurements (Blanco & McCarthy 1983), GJ93 favour $\mathrm{C/M} > 0.63$. However, M-giant spectral types are difficult to assess; we feel that it is safer to trust the C star counts, and admit that the number of M stars on the TP-AGB is not known, although it is probably greater than the number of O-rich LPVs – thus $\mathrm{C/M} \lesssim 0.6$. With t_M, t_S and t_C, the time spent by a star in the M, S and C phases, the C/M giants ratio on the TP-AGB is given by

$$\mathrm{C/M} = \frac{\int \mathrm{d}M\ \mathrm{SFR(M)} \times \mathrm{IMF(M)} \times \mathrm{t_C(M)}}{\int \mathrm{d}M\ \mathrm{SFR(M)} \times \mathrm{IMF(M)} \times \mathrm{t_M(M)}}, \tag{A10}$$

where the integral runs from $0.93\,\mathrm{M_\odot}$ to $\sim8\,\mathrm{M_\odot}$ (we kept the lower mass limit in GJ93). The M phase corresponds to $\mathrm{C/O} < 0.81$, the S phase to $0.81 < \mathrm{C/O} < 1$, and the C phase to $\mathrm{C/O} > 1$ (Smith & Lambert 1986). We followed GJ93 in neglecting obscuration of bright C stars due to excessive mass-loss. GJ93 also estimated that not more than 3 per cent of C stars brighter than $M_\mathrm{bol} = -6$ could have been missed by the optical

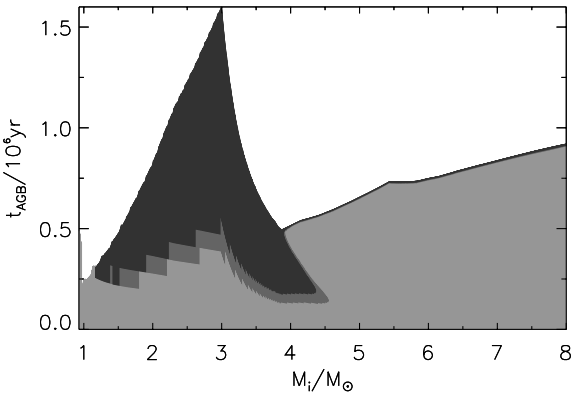

Figure A1. Time spent on the AGB (10^6 yr, in ordinates) as a function of initial mass, for the LMC model. The grey-scale grows darker from the M to S to C phases.

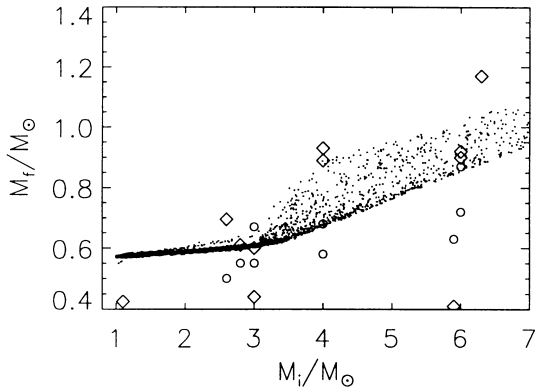

Figure A2. The initial–final mass relation from the Galactic model in this paper, and as observed. Diamonds and open circles correspond to final mass estimates based on surface gravity or stellar radius, respectively.

surveys. The functions t_M, t_S and t_C are shown in Fig. A1. The formula above, as well as the Monte Carlo runs, predict that M, S and C stars should occur in the ratio 0.65:0.04:0.31. This is a (TP-AGB) C/M star ratio of 0.47, in rough agreement with observations – provided that the observed ratio is indeed about 0.6; the LMC C/M star ratio on the TP-AGB is a rather uncertain quantity.

The observed LF of C stars in the LMC was reproduced from CF96. Fig. 5 gives examples of synthetic LFs that approximate the observed LF. The synthetic LFs were smoothed with a $\sigma = 0.2$ Gaussian, as in GJ93. Structure on small scales would not be picked up in observations anyway; there is considerable scatter about the bolometric correction law (CF96, their fig. 1). The distance modulus to the LMC was taken as 18.5.

As a note of caution, Marigo et al. (1999) have shown how the C-star LF is more sensitive to metallicity than it is to either the star formation history or the IMF. The metallicity dependence of the prescriptions we use also results in such a sensitivity, but an extrapolation from the LMC to the solar neighbourhood may seem far-fetched. It is assumed that none of the free parameters are metallicity-dependent.

A2.2 The initial–final mass relation

The initial–final mass for the 'standard' Galactic model is shown in Fig. A2, where it is compared to the data from Weidemann & Koster 1983 and Weidemann 1987 (data points from FC97). Final masses are derived from the surface gravity, or the stellar radius; there are thus sometimes two data points per object, with the same M_i. The agreement is satisfactory, except at low initial masses, where the model initial–final mass relation might be an overestimate (it should be kept in mind that the 'observed' initial–final mass relation is in fact model-dependent). Wagenhuber & Groenewegen (1998) reach the conclusion that the GJ93 approximations for the core masses at the first thermal pulse (which are used here, and largely determine the final mass) overestimated most other model results at low initial mass, but the discrepancy is small. The scatter in the model $M_i - M_f$ stems from the metallicity dependence of the analytical prescription for the core mass at the first thermal pulse (it is smaller for the prescription in Wagenhuber & Groenewegen 1998).

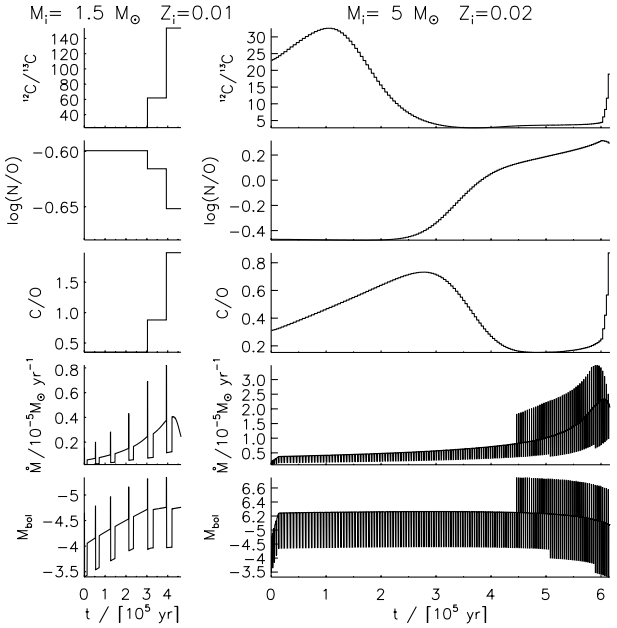

Figure A3. Synthetic evolution for characteristic initial masses. The results for the surface $^{12}C/^{13}C$, log(N/O), C/O, the mass-loss rate and bolometric absolute magnitude are shown from top to bottom, for initial masses 1.5 and 5 $M_\odot$ (from left to right).

A3 Evolution on the TP-AGB for characteristic initial masses

The synthetic AGB evolution of models with $(M_i, Z_i) = \{(1.5, 0.01); (5, 0.02)\}$ are shown in Fig. A3. The case with $M_i = 1.5\,M_\odot$ shows how towards the low-mass end of C-rich PNe progenitors, a low number of thermal pulses gradually builds up a ^{12}C surface overabundance. With $M_i = 5\,M_\odot$, the first $\sim 2 \times 10^5$ yr correspond to surface C enrichment, until core growth is high enough for T_B to reach CNO processing values. The total number of thermal pulses reaches 143, and at $t = 10^6$ yr the envelope mass drops below the adopted critical mass for the quenching of HBB.

This paper has been typeset from a TEX/LATEX file prepared by the author.